Ocean surface wind retrieval from copolarized SAR data using the polarization residual Doppler frequency

Faozi Saïd, *Student Member, IEEE* and Harald Johnsen

Abstract

An alternative approach to sea surface wind retrieval using SAR stripmap data is explored in this paper. The polarization residual Doppler frequency–the difference between the VV and HH Doppler centroids–(PRDF) is investigated as an additional key metric to the normalized radar cross section (NRCS). In order to successfully infer the wind field from the PRDF, the use of a geophysical Doppler model function, such as the GCM-Dop, is necessary. Using such function, a simulated version of the PRDF at X-band is analyzed in terms of the sea surface wind field at various incidence angles. Simulations first show that the PRDF increases with increasing incidence angle regardless of wind field conditions. Actual PRDF measurements also exhibit strong correlation with radial components of the wind speed. An alternate SAR wind retrieval procedure, incorporating both the PRDF and NRCS, is tested on a series of copolarized stripmap TerraSAR-X scenes carefully selected along the Norwegian coast. Both HH and VV NRCS are estimated on a 100 m x 100 m grid, while the VV and HH Doppler centroids on a 1 km x 1 km grid. Geophysical model functions used for this analysis are the GCM-NRCS and GCM-Dop. A 1.82 m/s bias, with a correlation of 0.79 and a 2.78 m/s RMSE, exist between the mean estimated wind speeds versus *in situ* measurements; while a 11.7 degree bias with a 0.9 correlation coefficient and a 39.89 degree RMSE are found between the mean estimated wind directions versus *in situ*.

Index Terms

Geophysical measurement techniques, Doppler measurements, sea surface, synthetic aperture radar

Funding for this work has been provided by the Troms County Regional Development fund (RDA).

I. INTRODUCTION

Sea surface wind retrieval using radar remote sensing devices is an inherently challenging and complex task. Scatterometer radars are the most common type of radar used thanks to their extensive spatial coverage and high orbital repeat rate. Wind information can be inferred from radar backscatter measurements using semi-empirical geophysical model functions (GMFs) tuned to radar specifications [1], [2], [3]. SAR instruments are an attractive alternative if very high resolution wind retrieval is preferred, or coastal winds are of interest. There are however two major obstacles in using such instruments: low orbital repeat rate and an infinite number of wind solutions for a given SAR backscatter measurement [4]. SAR streak detection has been explored as a way to help eliminate the underdetermined problem in wind retrieval [5], though such features are mostly detectable in high wind speed situations. [6] investigates the use of the Doppler centroid (D_c) combined with traditional radar backscatter measurements to help in ocean wind and current retrieval. In [7], the use of the Doppler centroid anomaly (the difference between the predicted geometric D_c and the measured D_c) at a given polarization, combined with NRCS and *in situ* information, is shown to improve wind direction retrieval. Such method is made possible by the use of a specifically developed GMF (CDop) which relates the Doppler centroid to the wind field [8]. Retrieving the wind field using the Doppler centroid at a single polarization is nonetheless a difficult task due to the nonlinear interactions of local wind with short and long waves, possible contribution from sea surface currents, and uncertainties in the predicted geometric D_c.

In this paper, we are investigating the use of the polarization residual Doppler frequency (PRDF), the difference between D_{cVV} and D_{cHH}, in a wind retrieval scheme using X-band data. Though the proposed method shares a few similarities with [7] and [9], it differs in the radar instrument, Doppler parameter, selected frequency band, and the GMFs used. The GMFs used for this study are based on the generalized curvature ocean surface scattering model (GCM) [10] [11]. Copolarized stripmap (SM) radar products are provided by the TerraSAR-X instrument. TerraSAR-X operates at 9.65 GHz at a nominal orbit height of 514 km at the equator, and provides 3.3 m azimuth and 1.7-3.49 m range resolution SM products at full performance within a 20 to 45 degree incidence angle range [12]. These specifications make TerraSAR-X a perfect candidate for this Doppler analysis.

This paper begins with a detailed analysis and simulation of the polarization residual Doppler frequency at X-band. Section three describes our wind retrieval scheme using the PRDF, in addition to commonly used sea surface wind retrieval methods. Section four provides a case study as well as some quantitative wind retrieval results using TerraSAR-X copolarized data. Section five concludes by discussing the potential of using the PRDF as a valid candidate in sea surface wind retrieval.

II. PRDF ANALYSIS BASED ON THE GCM-DOP

In this section, the PRDF is defined and simulated at X-band using the Doppler model from [11]. Simulation results are presented and discussed in order to determine the feasibility of using the PRDF in a wind retrieval scheme.

A. Definition

Predicting the Doppler centroid (D_c) on a stationary target is a straightforward procedure as described in the following equation

$$D_c = \frac{2V_s \sin\theta_{sq,c}}{\lambda}, \tag{1}$$

where V_s is the satellite inertial velocity, $\theta_{sq,c}$ is the squint angle at the beam center crossing time, and λ is the carrier signal's wavelength [13]. If the D_c is measured on a moving target, the target line-of-sight velocity needs to be taken into consideration for an accurate D_c estimation. Electromagnetic waves from SAR signals sent over the sea surface resonate with the short Bragg-scale waves as shown in the following equation

$$\lambda_s = \frac{\lambda_r}{2\sin\theta_i}, \tag{2}$$

where λ_r is the radar wavelength, λ_s is the short Bragg-scale waves wavelength, and θ_i is the incidence angle. These short waves may carry a certain velocity originated from three major sources: local wind stress, surface gravity waves, and surface currents. The resulting target velocity from these sources affects the Doppler centroid and is referred to as a wave orbital motion D_c contribution. This contribution is in contrast with the geometric D_c contribution shown in 1. We desire to highlight the wave orbital motion D_c contribution specifically originated from the local wind stress for wind retrieval purposes.

D_c contributions from geometry, possible electronic antenna mispointing, and surface currents must be eliminated or greatly reduced. This is made possible by computing the polarization residual Doppler frequency (PRDF) as shown in the following equation

$$\Delta D_c = D_{cVV} - D_{cHH}, \tag{3}$$

where ΔD_c represents the PRDF, D_{cVV} the Doppler centroid at the VV polarization, and D_{cHH} the Doppler centroid at the HH polarization (the polarization order in this operation is arbitrary). The PRDF computation allows the complete elimination of the geometric contribution to the D_c since the latter is polarization independent (see 1). It also allows a significant decrease in the mean surface current D_c contribution as it is considered zeroth-order Doppler frequencies [14], and therefore polarization independent as well. Using this metric requires however the use of copolarized SAR data.

B. Simulation analysis at X-band

A purely theoretical geophysical Doppler model function (GCM-Dop) has been developed to help infer sea surface wind speed and direction from Doppler centroid measurements [10] [11]. Since this model function simulates the convolution of the SAR signal with the ocean surface reflectivity, an ocean surface wave model must be used. Elfouhaily et al. [15] developed such model which has been integrated into the GCM-Dop. This geophysical Doppler model function, as shown in the following equation

$$D_c = G_{D_C}(\phi, U_{10}, \theta_i, f, pol, \gamma), \tag{4}$$

is designed to exclusively relate the wind field to the D_c contribution from the local wind stress only. In this equation, ϕ represents the wind direction relative to range, U_{10} represents the equivalent wind speed at 10 meters above the sea surface, θ_i is the incidence angle, f is the radar operating frequency, pol is the signal polarization, and γ represents an assumed inverse wave age. Fig. 1 illustrates how the D_c behaves using the GCM-Dop at both polarizations, for two different wind speeds given a 30 degree incidence angle and γ=0.84. It is also possible to simulate the PRDF in terms of the wind field in a similar manner. Fig. 2 shows the PRDF variation for 25, 30, and 36 degree incidence angles. These plots highlight some important features: the PRDF increases as θ_i increases; it is maximum in downwind and upwind (0 and 180 deg, respectively)

for any given wind speed and incidence angle; the PRDF is non-existent in the crosswind cases (90 and 270 deg); it monotonously decreases when the wind direction varies between 0 and 180 degrees while the opposite occurs between 180 and 360 degrees; given a wind direction, the absolute PRDF increases in terms of wind speed regardless of the incidence angle.

Fig. 3 shows how the PRDF varies in terms of the incidence angle in the upwind and downwind directions given 5 and 23 m/s wind speeds. It can be seen from this figure that in low incidence angle situations (i.e. less than 25 degrees) and especially at low wind speed, D_{cHH} and D_{cVV} are very close to each other leading to a PRDF in the order of a few Hertz. It is also important to note that low surface wind speed cases (e.g. below 3 m/s) combined with a moderately high incidence angle (i.e. above 35 degrees) may result in poor signal-to-noise ratio. Given the latter constraint, we conclude that the PRDF can be used in a wind retrieval process provided the incidence angle is less than 35 degrees, and the *in situ* wind speed is above 3 m/s.

As previously mentioned, the use of the GCM-Dop requires an assumed inverse wave age, the latter being a key component of the wave spectrum described in [15]. The PRDF simulation analysis discussed in this section is performed with γ=0.84 which corresponds to a fully developed sea. Fig. 4 shows how a +/- 10 % variation around the 0.84 value impacts the GCM-Dop performance; the PRDF standard deviation is plotted against the wind direction relative to range, given the same incidence angles as in Fig. 2 and a 23 m/s wind speed. From this figure, it can be seen that having γ=0.84 minimally impacts PRDF simulations (e.g. the maximum PRDF standard deviation in Fig. 2 found in upwind and downwind conditions is close to 3 Hz).

III. Wind retrieval method description

This section first elaborates on classical wind retrieval methods used by the scientific community. A wind retrieval scheme implementing PRDF observations is also introduced, where its advantages and limitations are discussed.

A. Classical methods

Currently used wind retrieval methods from radar backscatter signals require the use of geophysical model functions (GMFs), which relate the sea surface wind field to observed σ^o. This relationship can be expressed as follows

$$\sigma^o = G(U_{10}, \phi | \{f, pol, \theta_i\}), \tag{5}$$

where U_{10} is the wind speed, ϕ is the wind direction relative to range, f is the radar operating frequency, pol is the polarization state, and θ_i is the local incidence angle. Most GMFs are semi-empirical and adapted to a specific radar instrument: the Seawinds Ku-band scatterometer on QuikSCAT was used to measure σ^o over the sea surface and infer ocean wind vectors in near real time. NSCAT-2, QSCAT-1, QSCAT-1/F13 [3], and the latest Ku-2011 [16] are some of the GMFs specifically designed to be used with QuikSCAT data; the CMOD5.n GMF has been used with at least two different C-band scatterometers, namely ASCAT [1] and ERS-2 [2].

Regardless of the radar operating frequency band, observed σ^o oscillate in the wind direction domain as shown in the following equation

$$\sigma^o = B_0[1 + B_1 \cos(\phi) + B_2 \cos(2\phi)]^z, \tag{6}$$

where ϕ is the wind direction relative to range, the coefficients B_0, B_1, and B_2 are related to the wind speed, local incidence angle, polarization state, radar frequency, and the exponent z is a tuning parameter [4]. This inherent behavior leads to multiple wind solutions for each observed σ^o. Fig. 5 provides a 3D σ^o profile in terms of the wind field given γ=0.84, a 30 degree incidence angle, and HH polarization state at X-band (9.65 GHz). The GCM-NRCS, based on the generalized curvature ocean surface scattering model [10] [11], is used for this NRCS simulation. These multiple wind solutions are usually referred to as wind ambiguities. A finite set is obtainable when several σ^o measurements are performed on a given wind vector cell (wvc). Statistical techniques are used to reduce wind ambiguities and possibly find a single wind solution closest to the true wind. As an illustration, Seawinds on QuikSCAT performed several backscatter measurements from different azimuth looks on a given wvc where a maximum-likelihood estimator was implemented to solve for the true wind [3].

With SAR products, the problem becomes much more difficult to solve as a single σ^o measurement is available per wvc leading to an underdetermined problem. Since σ^o oscillates in the wind direction domain, while linear in the wind speed domain (see Fig. 5), most wind retrieval processes based on SAR products first solve for the wind direction prior to the wind speed [5] [17] [18]. Wind solutions can be inferred from SAR observations using GMFs developed for scaterrometers. Two major obstacles are however present as these model functions are usually designed for a single polarization (usually VV), and their respective resolution is coarse compared to standard SAR products. When co- or cross- polarized SAR observations are available, single

polarized simulated σ^o from GMFs must be converted. This procedure involves the use of a modeled polarization ratio (PR) [19] [20] as shown in the following equation

$$\sigma^o_{HH} = \sigma^o_{VVGMF} \cdot (\frac{\sigma^o_{HH}}{\sigma^o_{VV}})_{MODEL}. \tag{7}$$

B. Wind retrieval scheme using the PRDF

We are interested in incorporating PRDF observations into a SAR wind retrieval scheme in addition to standard σ^o observations. The major goal of this approach is to significantly reduce the wind ambiguity solution set without the use of ancillary data. It is important to note however that such scheme requires the use of copolarized SAR data as well as GMFs which can relate both Doppler centroid and NRCS observations to the wind field. Though the proposed method is similar to [7] and [9], it differs in the use of the PRDF instead of the Doppler centroid anomaly (i.e. the difference between the predicted geometric D_c and the measured D_c), as well as in the choice of geophysical Doppler model function; the method described in [7] and [9] use the semi-empirical CDop GMF [8], whereas we use the aforementioned GCM-Dop which supports both C- and X-band data.

In a given wvc, σ^o_{HH}, σ^o_{VV}, D_{cHH}, and D_{cVV} are first measured. Using these quantities and inverting the GCM-NRCS and GCM-Dop, we obtain the three following wind field functions

$$U_{10}(\phi|\{\sigma^o_{HH}, \theta_i, f, \gamma\}), \tag{8}$$

$$U_{10}(\phi|\{\sigma^o_{VV}, \theta_i, f, \gamma\}), \tag{9}$$

$$U_{10}(\phi|\{\Delta D_c, \theta_i, f, \gamma\}), \tag{10}$$

where U_{10} is the wind speed at 10 meters above the sea surface, ϕ is the wind direction relative to range, ΔD_c is the PRDF, θ_i is the incidence angle, f is the radar operating frequency, and γ is an assumed inverse wave age. An illustration of their corresponding curves is provided in Fig. 6 using two wvc from two different TerraSAR-X copolarized SM scenes. In each plot, two wind solutions are obtained by minimizing the following cost function

$$J = \sum_{j=HH}^{VV} \frac{\left(\sigma^o_{jM}(\underline{u}) - \sigma^o_{jOb}\right)^2}{\mathrm{Var}\left(\sigma^o_{jOb}\right)} + \frac{\left(\Delta Dc_M(\underline{u}) - \Delta Dc_{Ob}\right)^2}{\mathrm{Var}\left(\Delta Dc_{Ob}\right)}, \tag{11}$$

where $\mathrm{Var}\left(\sigma^o_{jOb}\right)$ and $\mathrm{Var}\left(\Delta Dc_{Ob}\right)$ represent the variances of the observed NRCS and PRDF values, $\sigma^o_{jM}(\underline{u})$ and $\Delta Dc_M(\underline{u})$ are the predicted NRCS and PRDF from the GCM-NRCS and

GCM-Dop, respectively, as a function of the wind field $\underline{u}$, σ^o_{jOb} and ΔDc_{Ob} are the observed NRCS and PRDF over a wvc, and the index j represents the polarization state. The following observations can be made from Fig. 6: the PRDF sign dictates whether the wind is blowing in the upwind (between 90 and 270 degrees) or downwind directions relative to the radar antenna (0 degree being downwind); if two wind solutions are obtained, they are not necessarily 180 degrees spread apart; when two wind solutions are found, they both share the same magnitude (i.e. wind speed); lower and upper limits on the wind speed are found given the observed NRCS alone (see 8 and 9); the number of wind ambiguities is greatly reduced by combining the use of the PRDF with observed NRCS without the use of ancillary data.

IV. PRDF WIND RETRIEVAL PROCESSING AND RESULTS

The following section describes the implementation of the wind retrieval scheme, mentioned in section III-B, with copolarized TerraSAR-X scenes. Results are compared against spatially and temporally collocated *in situ* measurements.

A. Process

The NRCS and Doppler centroid estimations are the first key steps to the wind retrieval process. Thanks to the high resolution of TerraSAR-X data, the selected cell size for NRCS estimation is 100 m x 100 m, while for D_c estimation 1 km x 1 km. As per TerraSAR-X instruction manual specifications [12], the NRCS estimation procedure requires a noise correction step regardless of the polarization state as follows

$$\sigma^o = (\langle |I_c|^2 \rangle - N) \sin \theta_i, \tag{12}$$

where I_c represents the complex intensity, $\langle\rangle$ is the sample mean operator, N represents the local calibrated noise power, and θ_i represents the local incidence angle.

The D_c estimation first consists of the azimuth Fourier spectrum estimation in each resolution cell and the use of a fitting procedure based on a Hanning window to determine the frequency at which the spectrum peaks (i.e. the D_c frequency). More details about the actual estimation method can be found in the Appendix. It is important to note that the standard TerraSAR-X SM product is not properly suited for precise azimuth Doppler centroid exploitation. This limitation is caused by the azimuth antenna pattern correction combined with the spectral weighting (Hanning

window) originally used in the TerraSAR-X Multimode SAR Processor [21]. Though a solution is proposed in [21], the dataset used in this paper (see Table I) does not benefit from it. Fig. 7 provides illustrations of both NRCS and D_c estimations for a 17 km x 56 km copolarized TerraSAR-X scene centered at lat 66.03/lon 8.09 acquired on 28 June 2010 at 1647 UTC. A blocking effect, caused by a block-wise processing of the TerraSAR-X SM data, is noticeable on the D_c estimation plots (see fourth, fifth and sixth plots of Fig. 7). This artifact somewhat disappears once the PRDF is computed (see sixth plot of Fig. 7).

Estimated NRCS and PRDF values are inputted into their respective GMF (GCM-NRCS and GCM-Dop) along with radar parameters to retrieve local wind information. Two wind solutions, both sharing the same wind speed, are obtained for each resolution cell. The wind vector solution containing the closest wind direction to *in situ* measurements is selected. A process summary is provided in the Appendix as a block diagram (see Fig. 12).

B. Case study

Fig. 8 shows the retrieved wind field corresponding to the TerraSAR-X scene used in Fig. 7. The estimated wind speed averaged over the whole scene is 7.6 m/s (with a standard deviation of 0.7 m/s) compared to an *in situ* measurement of 6.4 m/s; while the estimated wind direction is 232.7 degrees (with a standard deviation of 11.5 degrees) versus an *in situ* measurement of 218.8 degrees relative to range. *In situ* measurements were performed close to the scene center (lat 66.03/lon 8.09) within 15 minutes following the satellite pass. It is important to note that these measurements represent ten minute averages while the SAR measurements are considered instantaneous. Nonetheless, we can clearly see that both wind speed and direction estimates agree well with *in situ* measurements.

C. Quantitative results

A series of copolarized TerraSAR-X SM scenes are retrieved during the years 2008 and 2010 along the Norwegian coast in proximity to *in situ* weather stations (see Fig. 13 and table I for further details in the Appendix). *In situ* data are collocated within 30 minutes of each satellite pass, and a 160 km radius from each scene center. Most scene dimensions are around 17 km x 56 km. Each scene mean incidence angle varies between 23.4 and 32.7 degrees. Prior to implementing the estimated PRDF values from these scenes into our wind retrieval scheme,

correlation between estimated PRDF values and actual radial *in situ* wind speed is checked. For each scene, estimated PRDF values are averaged out over the whole grid to end up with a single value per scene. Fig. 9 shows estimated mean PRDF values versus radial *in situ* wind speed. This figure shows a clear correlation of 0.79 between these two metrics, and confirms the presence of the wind signature in the TerraSAR-X estimated PRDF.

The wind field is now estimated for each scene over a 100 m x 100 m grid using the wind retrieval scheme described in section III-B. On the left scatterplot of Fig. 10, the estimated wind speed averaged over each scene is plotted against the corresponding *in situ*. Error bars corresponding to the standard deviation are also plotted. Note a bias of 1.82 m/s which translates in slightly overestimated wind speeds; it is important to remind the reader that this scatterplot essentially compares instantaneous wind speed (i.e. the SAR measurement) versus a ten minute average (the *in situ* weather station measurement). A few results exhibit larger standard deviations, mostly due to the blocking effect described in subsection IV-A; this Doppler artifact can significantly change the estimated PRDF value and as a result negatively impact the wind field estimation. The right scatterplot of Fig. 10 provides a similar analysis for the wind direction component of the wind field. As mentioned in section III-B, two wind direction solutions are found in each resolution cell for each scene. For this analysis, the closest solution to the *in situ* wind direction is selected. The estimated wind direction is then averaged over the whole scene and compared to the *in situ* wind direction. The correlation between the two datasets is high (0.9) despite a large RMSE (39.89 deg). Though not readily apparent from this scatterplot, precise Doppler centroid measurement is fundamental for a reliable wind direction estimate, as a slight deviation in estimated PRDF can significantly alter results. These provided wind field results from Fig. 10 are nevertheless very promising.

V. Conclusion

In this paper, the potential use of the polarization residual Doppler frequency (PRDF) as a key metric in a sea surface wind retrieval scheme has been explored. PRDF simulation analysis is provided based on a geophysical Doppler model function (GCM-Dop) at X-band. This analysis leads to the following results: the absolute Dc_{HH} is always greater (except in crosswinds) than Dc_{VV} regardless of incidence angle and wind field conditions; their difference is maximum in upwind and downwind and zero in crosswinds; for a given wind direction, the PRDF increases

as the incidence angle increases regardless of the wind speed; for any given wind speed and incidence angle, the PRDF varies monotonously between upwind and downwind; a +/-10 % variation around γ=0.84 minimally impacts the PRDF; finally X-band SAR sea surface wind retrieval using the PRDF should be avoided above 35 degree incidence angle combined with low wind speed, due to possible poor signal-to-noise ratio.

A new wind retrieval scheme is also introduced in this paper, where σ^o_{hh}, σ^o_{vv}, ΔD_c = D_{cVV}-D_{cHH} are the input variables to two geophysical model functions (GCM-NRCS and GCM-Dop). By inverting these GMFs and minimizing an appropriate cost function, two wind solutions are found given a set of σ^o_{hh}, σ^o_{vv}, and ΔD_c measurements. These two wind solutions share the same wind speed while their respective wind direction are not necessarily 180 degrees apart. Furthermore, both wind solutions are either upwind or downwind depending on the PRDF sign. To validate such wind retrieval method, 19 copolarized SM TerraSAR-X scenes ($\sim$17 km x 56 km) have been carefully selected along the Norwegian coast in close proximity to *in situ* weather stations. σ^o_{hh} and σ^o_{vv} are both estimated on a 100 m x 100 m grid for each scene, while D_{cHH} and D_{cVV} are estimated on a 1 km x 1 km grid. Mean estimated wind speed over each scene agree well with their respective collocated *in situ* weather stations. The same can be said of the wind direction component, though sudden PRDF variation can significantly alter wind direction estimates. Therefore precise Doppler centroid estimation is key for successfully retrieving the wind field from SAR data using both NRCS and PRDF.

Although promising results are obtained using the above mentioned GMFs, improvements can be made with the current version of the geophysical Doppler model function used in this study (GCM-Dop). The GCM-Dop currently provides equal D_c values in upwind and downwind regardless of incidence angle, γ, polarization, wind speed, and radar operating frequency. Using a different geophysical Doppler model function (Cdop), [7] shows that absolute D_c measurements are in fact greater in upwind than downwind regardless of incidence angle and wind speed. Furthermore, while scattering from breaking waves has been incorporated into the GCM-NRCS [20], it has not yet been implemented into the current version of the GCM-Dop. Such implementation into the GCM-Dop should help in obtaining greater absolute D_c values in upwind compared to downwind.

The sea surface description used for both GCM based GMFs is able to provide Stoke like waves description, but fails in offering any skewness factor. Future works are currently planned

to enable such features which will eventually bring a more realistic sea surface description, and improve the GMFs performance. Finally, we have claimed that the PRDF estimation is able to significantly decrease possible surface current D_c contribution. Further analysis, where surface current D_c contribution can be quantified, are needed to confirm and validate such claim.

VI. Appendix

A. D_c estimation description

In this appendix, the Doppler centroid estimation method implemented in this study is briefly described. The primary step is carefully deciding the size of a resolution cell within a given scene (e.g. 1 km x 1 km). Each of these cells are subsequently broken down into N smaller blocks (256 pixels x 256 pixels with a 50 % overlap). Let slc be an array variable corresponding to the single look complex data found in a given block. A fast Fourier transform is applied to slc over each azimuth line, summed up over the whole block range, and finally averaged out to obtain the block azimuth magnitude spectrum. Equation 13 summarizes this first step as follows

$$S_{blk} = \frac{1}{256} \sum_{i=1}^{256} |FFT(slc[i,:])|, \tag{13}$$

where i represents the range index, FFT represents the Fast Fourier Transform operation, : returns all azimuth indices, and S_{blk} represents the resulting azimuth magnitude spectrum for a given 256 pixels x 256 pixels block.

The resulting azimuth magnitude spectrum for a 1 km x 1 km cell, S_{cell}, is found by computing the sample mean of all S_{jblk} found within the cell, as follows

$$S_{cell} = \frac{1}{N} \sum_{j=1}^{N} S_{jblk}. \tag{14}$$

Fig. 11 illustrates such spectrum. Note that for a better side-lobe suppression, spectral weighting is applied to both range and azimuth spectra as part of the TerraSAR-X Multimode SAR Processor [12]. In order to determine the Doppler centroid from S_{cell}, a Hanning window is shifted around the peak of S_{cell} at an arbitrary rate of 0.4 Hz, and the linear Pearson correlation coefficient between the two spectra is computed at each shift. The D_c is found when the correlation coefficient is highest. This procedure is then repeated for each 1 km x 1 km cell over a given scene.

B. Additional wind retrieval scheme information

Fig. 12 provides a block diagram which summarizes the wind retrieval scheme described in this paper. Table I and Fig. 13 provide further information regarding the dataset used in this study. It also includes information about the collocated *in situ* data. The provided latitude and longitude coordinates in table I point to each scene center location. The *in situ* distance refers to the distance between the scene center and the *in situ* weather station location. Finally, the provided incidence angle (θ_i) in Table I corresponds to the scene center's incidence angle.

REFERENCES

[1] Ocean and S. I. SAF, *ASCAT Wind Product User Manual*, KNMI, De Bilt, the Nertherlands, August 2011. [Online]. Available: http://www.knmi.nl/scatterometer/publications/pdf/ASCAT_Product_Manual.pdf

[2] K. E. Team, *ERS Scatterometer Product User Manual*, KNMI, De Bilt, the Nertherlands, November 2008. [Online]. Available: http://www.knmi.nl/scatterometer/publications/pdf/ERS_Product_Manual.pdf

[3] T. Lungu, *QuikSCAT Science Data Product User's Manual: Overview and Geophysical Data Products, version 3.0*, Jet Propulsion Lab., Pasadena, Calif., June 2006. [Online]. Available: ftp://podaac.jpl.nasa.gov/pub/ocean_wind/quikscat/doc/QSUG_v3.pdf

[4] M. P. Arnús, "Wind field retrieval from satellite radar systems," Astronomy and Meteorology Department, University of Barcelona, September 2002.

[5] J. Horstmann and W. Koch, "Measurement of ocean surface winds using synthetic aperture radars," *Oceanic Engineering, IEEE Journal of*, vol. 30, no. 3, pp. 508 –515, july 2005.

[6] B. Chapron, F. Collard, and F. Ardhuin, "Direct measurements of ocean surface velocity from space: interpretation and validation," *Journal of Geophysical Research*, vol. 110, no. C07008, 2005, doi:10.1029/2004JC002809.

[7] A. A. Mouche, F. Collard, B. Chapron, K.-F. Dagestad, G. Guitton, J. A. Johannessen, V. Kerbaol, and M. W. Hansen, "On the use of doppler shift for sea surface wind retrieval from sar," *Geoscience and Remote Sensing, IEEE Transactions on*, vol. 50, no. 7, pp. 2901–2909, July 2012.

[8] F. Collard, A. A. Mouche, B. Chapron, C. Danilo, and J. Johannessen, "Routine high resolution observation of selected major surface currents from space," in *Proceedings of SEASAR 2008, SP-656*. ESA - ESRIN, Frascati, Italy: ESA, 2008. [Online]. Available: http://earth.esa.int/seasar2008/participants/287/pres_287_Collard.pdf

[9] K. F. Dagestad, A. Mouche, F. Collard, M. W. Hansen, and J. A. Johannessen, "On the use of Doppler shift for SAR wind retrieval," in *3rd Int. Workshop SeaSAR*, 2010, pp. 1–8.

[10] G. Engen, I. Friestad-Pedersen, H. Johnsen, and T. Elfouhaily, "Curvature effects in ocean surface scattering," *IEEE Transactions on Antennas and Propagation*, vol. 54, no. 5, pp. 1370–1379, May 2006.

[11] I. F. Pedersen, G. Engen, and H. Johnsen, "Polarization dependency in sea surface doppler frequency and its application to envisat asar alt-pol data," in *Envisat and ERS Symposium*. Norut Information Technology, September 2004.

[12] M. Eineder, T. Fritz, J. Mittermayer, A. Roth, E. Borner, and H. Breit, *TerraSAR-X Ground Segment Basic Product Specification Document*, German Aerospace Center (DLR), Germany, October 2010.

[13] I. G. Cumming and F. H. Wong, *digital processing of SYNTHETIC APERTURE RADAR DATA*. ARTECH HOUSE, 2005, ch. Doppler Centroid Estimation.

[14] R. Romeiser and D. R. Thompson, "Numerical study on the along-track interferometric radar imaging mechanism of oceanic surface currents," *IEEE Transactions on Geoscience and Remote Sensing*, vol. 38, no. 1, pp. 446–458, 2000.

[15] T. Elfouhaily, B. Chapron, K. Katsaros, and D. Vandemark, "A unified directional spectrum for long and short wind-driven waves," *Journal of Geophysical Research - Oceans*, vol. 102, no. C7, pp. 15,781–15,796, 1997.

[16] L. Ricciardulli and F. Wentz, "Reprocessed quikscat (v04) wind vectors with ku-2011 geophysical model function," Remote Sensing Systems, Tech. Rep., April 2011. [Online]. Available: http://www.ssmi.com/qscat/qscat_Ku2011_tech_report.pdf

[17] C. Wackerman, C. Rufenach, R. Shuchman, J. Johannessen, and K. Davidson, "Wind vector retrieval using ers-1 synthetic aperture radar imagery," *Geoscience and Remote Sensing, IEEE Transactions on*, vol. 34, no. 6, pp. 1343 –1352, nov 1996.

[18] T. Bergeron, M. Bernier, K. Chokmani, A. Lessard-Fontaine, G. Lafrance, and P. Beaucage, "Wind speed estimation using

polarimetric radarsat-2 images: Finding the best polarization and polarization ratio," *Selected Topics in Applied Earth Observations and Remote Sensing, IEEE Journal of*, vol. 4, no. 4, pp. 896 –904, dec. 2011.

[19] A. Mouche, D. Hauser, J.-F. Daloze, and C. Guérin, "Dual polarization measurements at C-band over the ocean: Results from airborne radar observations and comparison with ENVISAT ASAR data," *IEEE Transactions on Geoscience and Remote Sensing*, vol. 43, pp. 753–769, 2005.

[20] H. Johnsen, G. Engen, and G. Guitton, "Sea-surface polarization ratio from envisat asar ap data," *IEEE Transactions on Geoscience and Remote Sensing*, vol. 46, no. 11, pp. 3637–3646, November 2008.

[21] C. Rossi, H. Runge, H. Breit, and T. Fritz, "Surface current retrieval from terrasar-x data using doppler measurements," in *Geoscience and Remote Sensing Symposium (IGARSS), 2010 IEEE International*, july 2010, pp. 3055 –3058.

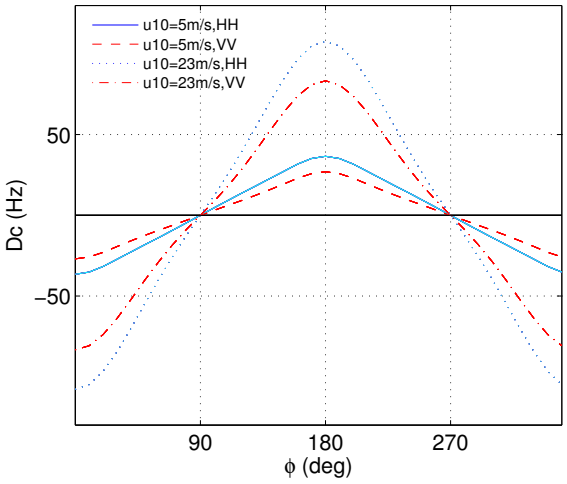

Fig. 1. Plots of HH and VV Doppler centroids vs. wind direction relative to range, for two different wind speeds (5 and 23 m/s). Note the D_c extrema in downwind and upwind (0 and 180 degrees, respectively), and zeros in crosswinds (90 and 270 degrees). These plots are performed using the GCM-Dop given f=9.65 GHz, θ_i=30 deg, and γ=0.84.

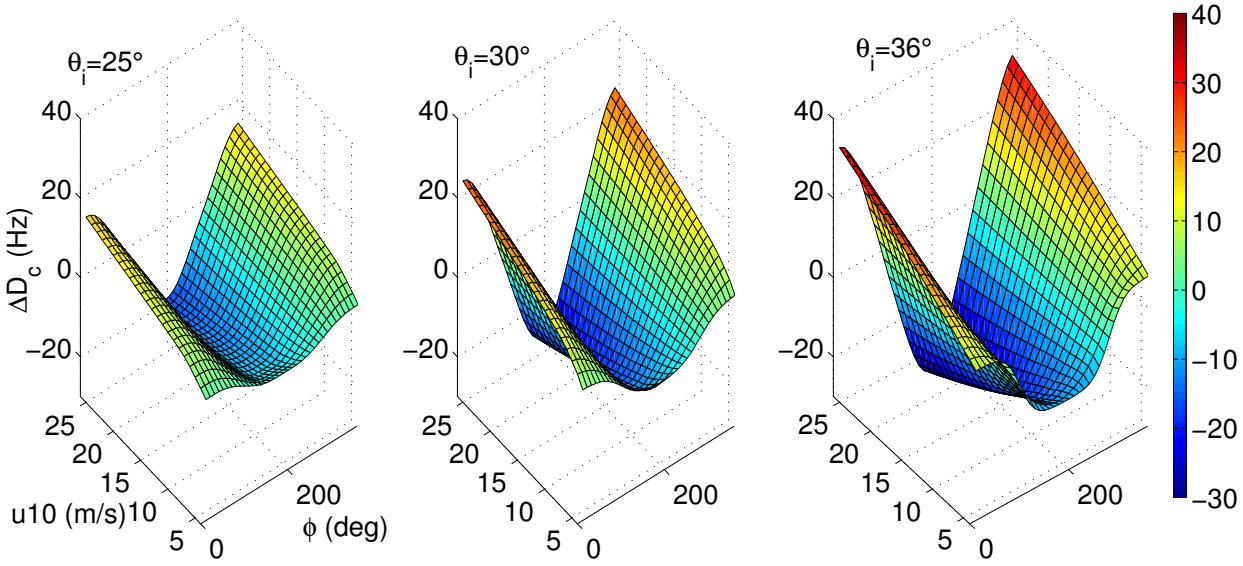

Fig. 2. 3D PRDF representations in terms of the wind field for three different incidence angles (25, 30, and 36 deg), given γ=0.84 at X-band (9.65 GHz). Some of the key PRDF characteristics shown here are its increase as the incidence angle or the wind speed increase; PRDF extrema are found in upwind and downwind conditions (180 and 0 deg, respectively); a monotonous decrease as the wind direction varies between 0 and 180 degrees while the opposite occurs between 180 and 360 degrees.

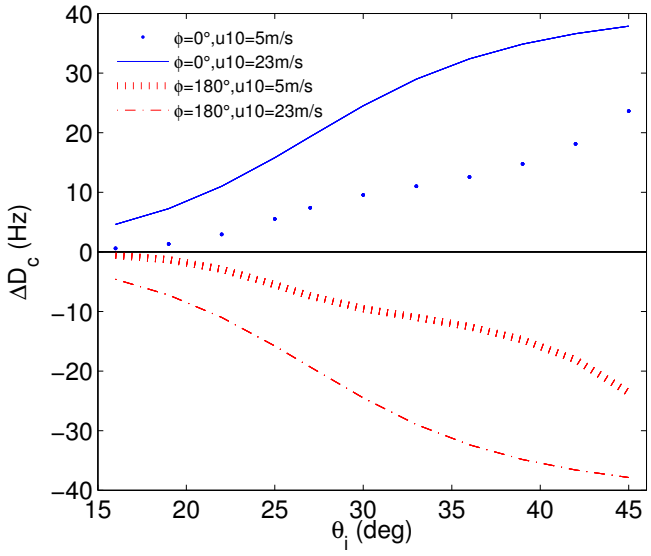

Fig. 3. This plot shows the PRDF variation in terms of the incidence angle in upwind and downwind conditions for 5 and 23 m/s wind speeds. Below 25 degree incidence angle, the absolute PRDF is less than 15 Hz for both low and high wind speed cases (i.e. the distinction between D_{cHH} and D_{cVV} is minimal). This simulation is done using the GCM-Dop with f=9.65 GHz and γ=0.84. ϕ=0^o corresponds to downwind while ϕ=180^o to upwind.

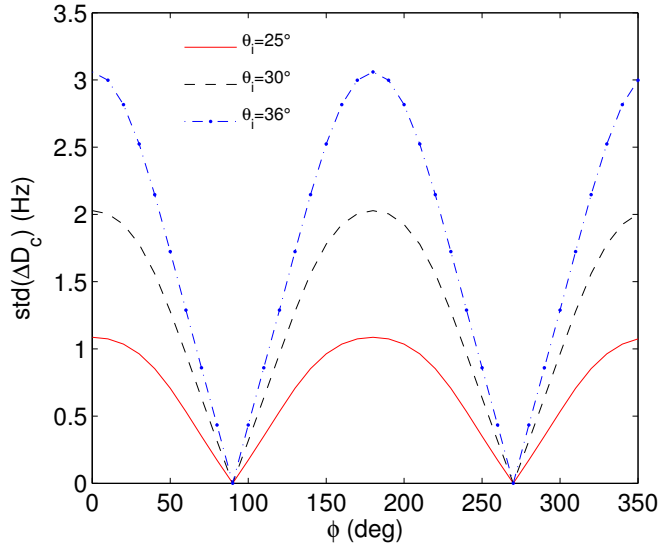

Fig. 4. Plot showing the impact of a +/-10 % variation around γ=0.84 on the PRDF given a 23 m/s wind speed and three different incidence angles. Though the γ impact on the PRDF is greater with a larger incidence angle, the effect is minimal (less than 3 Hz). Note that ϕ=0^o corresponds to downwind while ϕ=180^o to upwind.

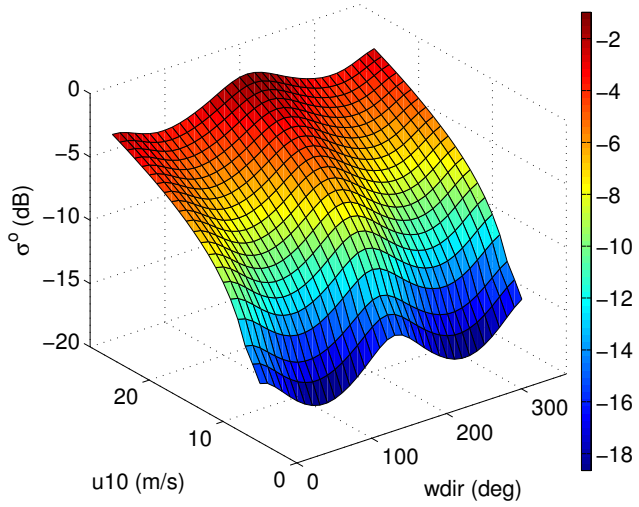

Fig. 5. 3D NRCS representation in terms of the wind field given γ=0.84, a 30 degree incidence angle, and HH polarization at X-band (9.65 GHz). Note the oscillatory behavior of σ^o, thereby leading to multiple wind solutions for a given σ^o measurement. This NRCS simulation is based on the GCM-NRCS GMF [10] [11].

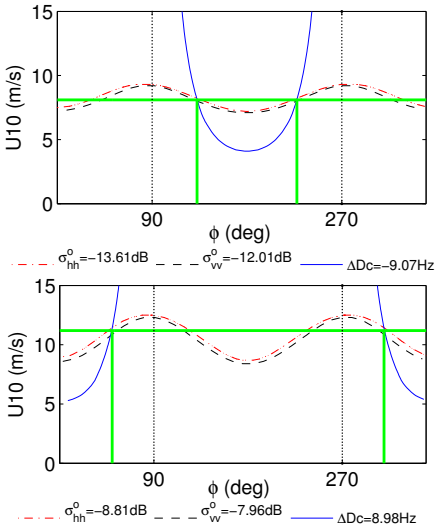

Fig. 6. Cost function minimization applied on two wvc from two different TerraSAR-X scenes. Each curve shows the wind speed variation in terms of the wind direction for each σ^o_{HH}, σ^o_{VV}, and ΔD_c measurement provided in the legends (see 8, 9, and 10). In each plot, note the two wind solutions (shown where the green lines intersect) sharing the same wind speed. These two solutions are not necessarily 180 degrees apart. The PRDF sign dictates if the wind is upwind or downwind w.r.t the radar antenna.

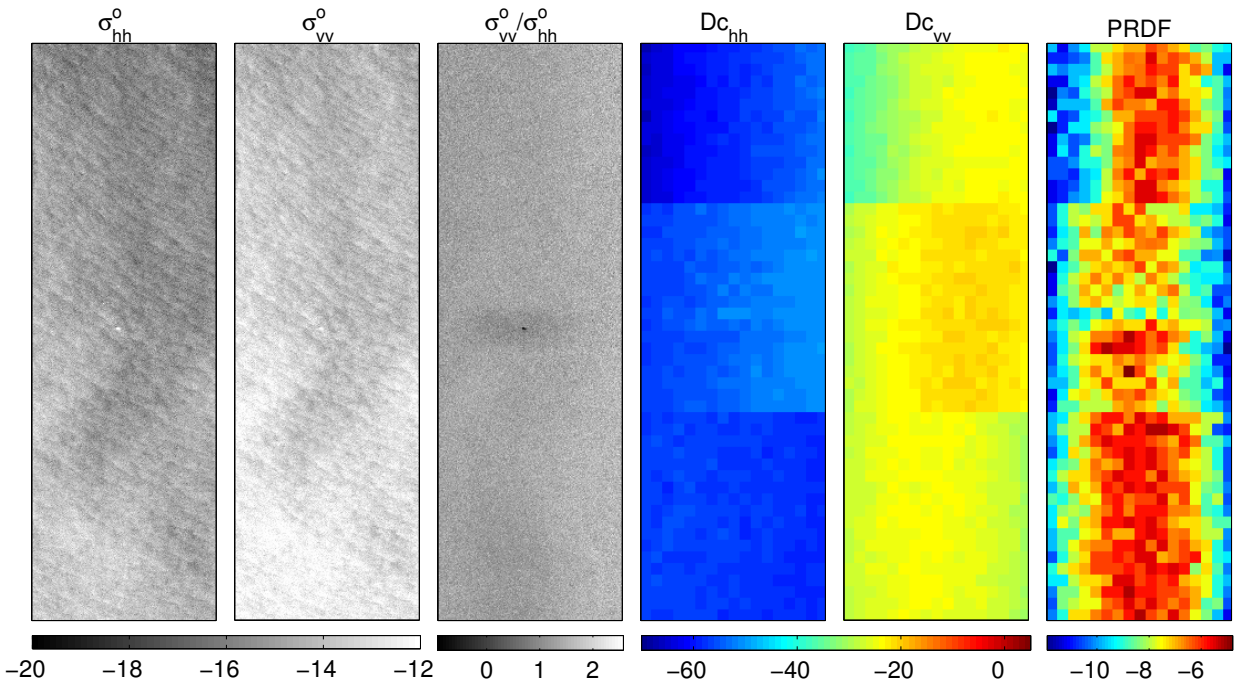

Fig. 7. 2D NRCS and D_c representations of a 17 km x 56 km copolarized SM TerraSAR-X scene retrieved on 28 June 2010 at 1647 UTC, centered at lat 66.03/lon 8.09. The two most left plots represent 2D NRCS at HH and VV polarizations, respectively; the third plot shows the corresponding polarization ratio ($\sigma^o_{vv}/\sigma^o_{hh}$); the fourth and fifth plots represent 2D D_c profiles at HH and VV polarizations, respectively; the right most plot shows the corresponding PRDF. The mean incidence angle at the scene retrieval time was 32.73 degrees. Scales for NRCS and D_c figures are in dB and Hz, respectively.

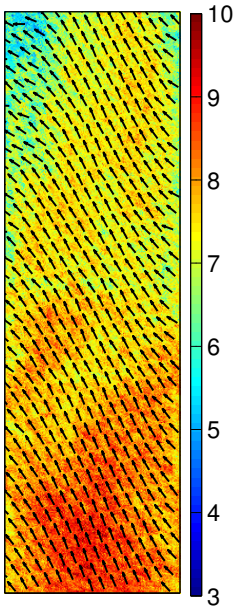

Fig. 8. 2D wind field corresponding to the TerraSAR-X scene shown in Fig. 7. *In situ* weather station is located close to the scene center. Provided *in situ* wind speed is 6.4 m/s, and wind direction 218.8 degrees. These measurements are performed within the next fifteen minutes of the satellite pass. Mean estimated wind speed is 7.6 m/s with a 0.7 m/s standard deviation, and mean estimated wind direction is 232.7 degrees with a 11.5 degrees standard deviation. Colorbar is in m/s. Provided wind direction measurements are relative to range, with 0^o being downwind.

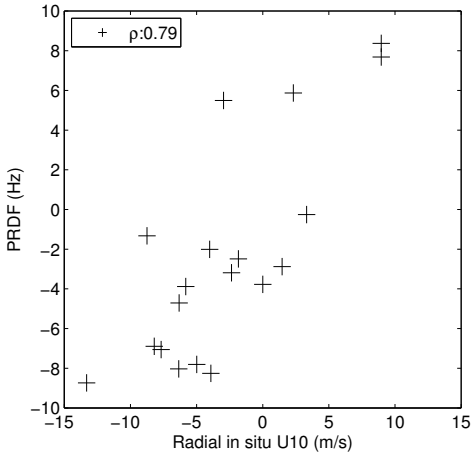

Fig. 9. Plot of the estimated PRDF (mean value over each whole scene) versus radial *in situ* wind speed. A correlation of 0.79 is shown between the two metrics proving that the wind signature is definitely present in the PRDF.

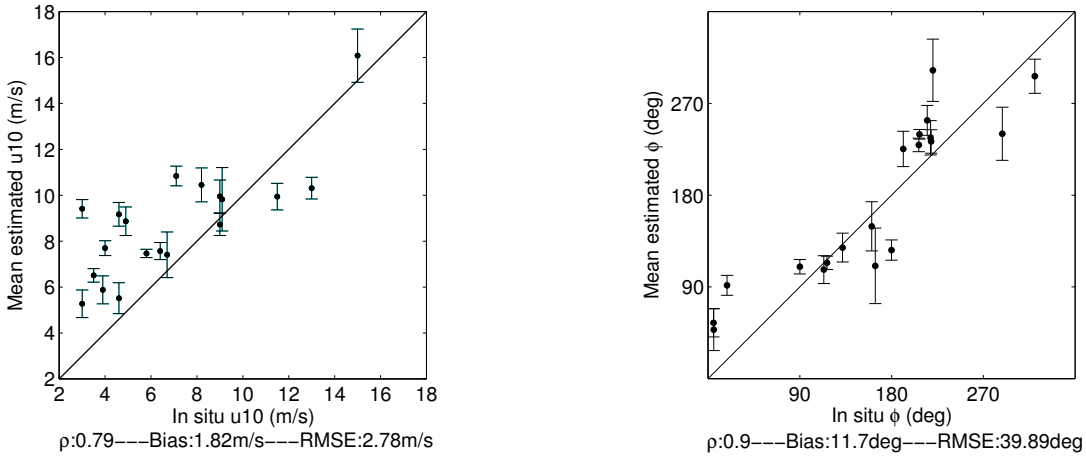

Fig. 10. Plots of the estimated wind field from each of the selected copolarized TerraSAR-X SM scenes along the Norwegian coast. The scatterplot on the left shows the mean estimated versus *in situ* wind speeds. Estimated wind speeds are averaged out over each respective scene. Error bars corresponding to standard deviations are also included. Note a 1.82 m/s bias pointing to slightly overestimated wind speeds compared to *in situs*. The scatterplot on the right shows the corresponding wind direction results versus *in situ*. The correlation between the two datasets is high (0.9) despite a 39.89 degree RMSE.

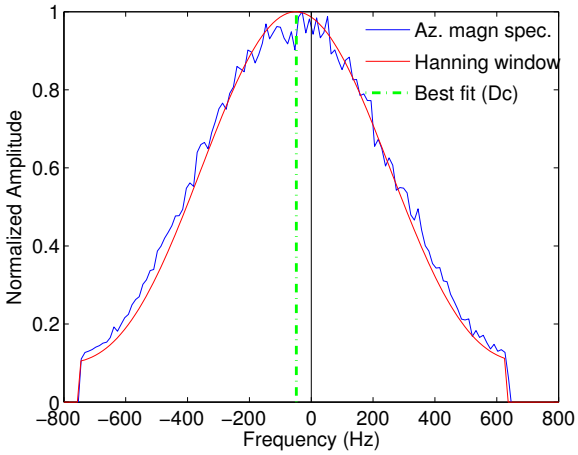

Fig. 11. Azimuth magnitude spectrum of a 1 km x 1 km cell, overlaid with a Hanning window. The latter has a 0.6 width parameter as per TerraSAR-X instruction manual specifications [12]. The D_c is found by finding the best fit of the Hanning window to the azimuth spectrum.

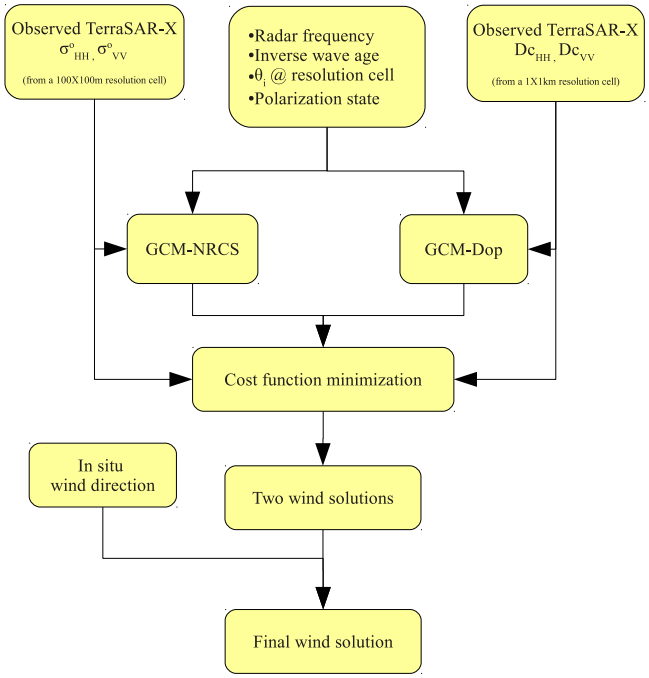

Fig. 12. Block diagram summarizing our wind retrieval process using TerraSAR-X SM copolarized data with both the GCM-Dop and GCM-NRCS GMFs. Observed σ^o_{hh}, σ^o_{vv}, and PRDF values from a given resolution cell are inputted into their respective GCM based GMF. Radar parameters are also necessary to properly tune both GMFs. A cost function minimization is then performed to find the corresponding two wind solutions which only differ in their direction. *In situ* wind direction is used to select the closest wind solution to ground truth.

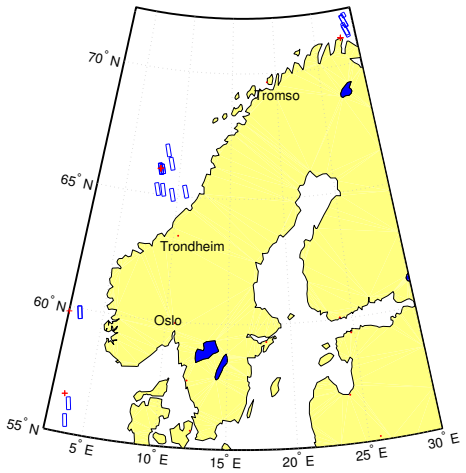

Fig. 13. Map showing the various satellite passes (blue rectangles) used in this wind retrieval study; a total of 19 scenes along the Norwegian coast have been carefully selected in proximity to weather stations (shown with red crosses). Further details regarding exact *in situ* locations and scenes can be found in table I.

TABLE I

TERRASAR-X DATASET USED IN THIS STUDY, ALONG WITH COLLOCATED *in situ* WEATHER STATION INFORMATION

Date	Time (UTC)	Ins time (UTC)	θ_i (deg)	Cent lat	Ins lat	Cent lon	Ins lon	Ins dist (km)	Station Name
2008/04/22	15:05	15:00	31.7	71.95	71.08	29.13	28.22	101.1	Gamvik
2008/04/19	05:02	05:00	29.4	71.39	71.08	29.01	28.22	44.3	Gamvik
2008/04/22	15:05	15:00	29.4	71.31	71.08	29.03	28.22	38.4	Gamvik
2008/05/03	15:05	15:00	30.6	71.70	71.08	29	28.22	74.2	Gamvik
2008/04/30	05:02	05:00	30.6	71.72	71.08	28.98	28.22	76.3	Gamvik
2010/06/05	06:13	06:00	23.4	66.26	66.03	9.13	8.09	53.9	Norne
2010/06/07	16:30	16:00	23.4	65.21	66.03	10.73	8.09	152.9	Norne
2010/06/01	16:38	17:00	27.1	65.03	66.03	9.5	8.09	128.7	Norne
2010/05/30	17:11	17:00	24.7	59.84	59.80	3.15	2.3	47.9	Heimdal
2010/07/04	16:39	17:00	24.6	66.02	66.03	8.31	8.09	10.3	Norne
2010/06/12	16:39	17:00	24.6	66.02	66.03	8.31	8.09	10.5	Norne
2010/06/16	06:13	06:00	27.1	66.01	66.03	8.12	8.09	2.0	Norne
2010/06/27	06:13	06:00	27.1	66.02	66.03	8.12	8.09	2.0	Norne
2010/06/28	16:47	17:00	32.7	66.03	66.03	8.1	8.09	0.5	Norne
2010/06/16	06:16	06:00	24.6	56.19	56.55	3.65	3.25	47.2	Ekofisk
2010/06/15	17:19	17:00	29.4	55.50	56.55	3.62	3.25	119.1	Ekofisk
2010/08/17	16:38	17:00	20.9	65.20	66.03	8.04	8.09	92.3	Norne
2010/08/21	06:13	06:00	27.1	66.78	66.03	8.64	8.09	87.2	Norne
2010/08/22	16:47	17:00	32.7	65.19	66.03	8.57	8.09	95.1	Norne